STM JOURNALS

Journal of
Polymer & Composites

ISSN: 2321-2810 (Online)
ISSN: 2321-8525 (Print)
Volume 14, Special Issue 2, 2026
DOI (Journal): 10.37591/JoPC

https://journals.stmjournals.com/jopc

Research JoPC

Water Chestnut Stem-Derived Biochar Supported AgNPs/AC-CTS-PVA Composite Gel for Wastewater Treatment and Potent Antibacterial Performance

Mohattib Ali[1], Deepak Kumar[2] , Pramendra Kumar[3,*]

Abstract

In the present study, green and efficient Ag-NPs functionalized activated carbon/chitosan-polyvinyl alcohol (AgNPs/AC-CTS-PVA) composite gel was successfully synthesized using water chestnut stem-derived biochar for wastewater treatment and antibacterial applications. The composite was characterized by FTIR, XRD, SEM-EDX, and TGA analyses, confirming the successful incorporation of crystalline Ag nanoparticles within the polymeric matrix and improved thermal stability. The material was tested regarding the removal of the dye of methylene blue (MB) under different conditions of the experiment. The optimum dye removal rate reached 98% at pH 7 when 20 mg adsorbent dose was used within 60 min, kinetic modeling of the adsorption reaction was performed that the reaction adhered to the Elovich model (R^2 = 0.9622), which means it was heterogeneous surface chemisorption, and intra-particle diffusion was also a significant contributor to the isotherm analysis indicated a very good fit to the Langmuir model (R^2 = 0.9938) with a maximum adsorption capacity ($Q_{\square}$) of 106.38 mg g^{-1}, indicating that the adsorption occurred in a monolayer fashion. Furthermore, the composite exhibited remarkable antibacterial activity against Staphylococcus aureus and Pseudomonas aeruginosa, producing a 38 mm and 36 mm inhibition zone, comparable to penicillin (42 mm). The findings demonstrate that the synthesized AgNPs/AC-CTS-PVA gel is a promising multifunctional material for sustainable wastewater remediation and antimicrobial applications.

Keywords: Activated carbon, chitosan, silver nanoparticles, antibacterial, dye adsorption

INTRODUCTION

Water pollution is a very serious environmental issue for the whole world, and its rate is increasing rapidly. Water contamination affects directly or indirectly a billion or more people in the world. Clean and unpolluted water is not only necessary for drinking, but also in other areas of life. Several of these contaminants include noxious heavy metals, dyes, pesticides, fertilizer, degraded organic contaminants, pharmaceutical wastes and other organic and inorganic materials, which are present in large quantities in polluted water [1, 2]. Polluted water can also act as a carrier of diseases and this is a big danger for human health. This plays a vital role the treatment of sewage using safe bacteriostatic material in an effective method. Based on the pH concentration of various water sources, there is dire need to develop antibacterial materials that can be used under varying water conditions and possess good bacterio-static properties [3]. *Trapanatans L.* (also called water chestnut or Singhada (Hindi) is a free-floating, perennial aquatic plant that is widely grown and

***Author for Correspondence**
Pramendra Kumar

[1]Research Scholar, Department of Applied Chemistry, M.J.P. Rohilkhand University, Bareilly, Uttar Pradesh, India
[2]Assistant Professor, Department of Chemistry, Constituent Government College Richa Baheri, MJPRU Bareilly, Uttar Pradesh, India
[3]Associate Professor, Department of Applied Chemistry, M.J.P. Rohilkhand University, Bareilly, Uttar Pradesh, India

Received Date: April 13, 2026
Accepted Date: April 20, 2026
Published Date: May 10, 2026

Citation: Mohattib Ali, Deepak Kumar, Pramendra Kumar. Water Chestnut Stem-Derived Biochar Supported AgNPs/AC-CTS-PVA Composite Gel for Wastewater Treatment and Potent Antibacterial Performance. Journal of Polymer & Composites. 2026; 14(Special Issue 2): S1129–S1144p.

eaten in Asia and especially in India, China, and the Southeast Asian nations. Water chestnut flourishes in slow moving or stagnant fresh water bodies like lakes, ponds and marshlands. The plant is an aquatic plant that produces edible and starchy fruits that are very useful in nutrition and treatment [4]. The oil obtained out of the fruits has been used as a medicine of rheumatism, sores and sunburn. Cancer preventing properties have also been reported in trapanatans. Stem is administered in the form of juice for eye diseases. Clearing summer-heat, allaying fever, diffusing dampness and dispelling pathogenic wind and invigorating the spleen, etc. are some of the other uses. It has already been reported that several biological activities such as analgesic, anti-inflammatory, antidiabetic and antimicrobial activity have been reported in various parts of Trapanatans L [5]. In the recent past, biochar material has become a prospective adsorbent due to its availability, hydrophobic surface, layered pore structure, environmental friendliness, cost efficiency, thermal stability, multi functional groups and modification ease. Biochar is a carbonaceous substance that is highly aromatic and formed due to the incomplete combustion of raw materials at high temperature in the presence of limited oxygen [6]. Activated carbon (AC) has a well developed porous structure and great surface area, diverse chemical functional groups, high adsorption capacity, recyclability features, and chemical stability, and is applied in purifying waste water [7]. According to K. Senthilkumar, the methylene blue dye is a widely used in adsorption research since it is a model pollutant that is used to represent an organic contaminant that is commonly present in wastewater. It is a commonplace method of measuring performance of adsorbents such as activated carbon due to its wide usage in research. Methylene blue has a rather simple molecular structure, which enables it to react with the surface of activated carbon. This renders it a useful test dye in the investigation of adsorption capacity of carbon materials and the mechanisms. Among them, the most famous and effective method is adsorption that involves using porous carbonaceous materials, such as activated carbon [8]. Silver nanoparticles have a broad range of applications including antibacterial agents, sensors and biomedical applications. Green synthesis of silver nanoparticles helps in the elimination of the dangerous reagents at every stage that leads to environmental friendly synthesis of silver Nanoparticles [9]. Currently silver nanoparticles (AgNPs) that have high antibacterial potential have been employed in the study and application of antibacterial materials. AgNPs are regarded as one of the strongest and safest antibacterial agents. They possess a good antibacterial action against numerous bacteria, fungi and viruses [10]. Chitosan (CTS) has good properties like non-poisonous, biocompatibility, biodegradable and non-carcinogenicity. Thus, chitosan can be used various applications such as biomedicine, antimicrobial agent, wastewater treatment, food packaging, functional membranes, flocculation [11]. CTS is a natural biostatic agent. CTS and its derivatives possess good antibacterial activity and are capable of inhibiting the growth and reproduction of fungi, bacteria and viruses CTS is readily dissolved in a weak acid solution and the dissolved solution has amino groups that prevent the growth of bacteria by binding themselves the a negative charge on the surface of the bacterial cell membrane [12]. Polyvinyl alcohol (PVA) is a water soluble, semi crystalline, non-toxic and eco-friendly, as well as heat stable synthetic biopolymer [13]. The reports concerning the use of PVA-based materials in food packaging, drug delivery, wound dressing, and removal of contaminants dyes and heavy metal ions in wastewater are numerous. PVA is hydrophilic and commonly employed to entrap bacteria and bacteriostatic agents [3]. The polyvinylpyrrolidone (PVP) or povidone is a synthetic polymer, a product of radical polymerisation of vinylpyrrolidone monomers, first reported in 1939 by the German scientist Walter J. Reppe. The application of PVP is popular in the biomedical, pharmaceutical, water purification, and other applications due to its distinctive characteristics, e. g., solubility, adhesive, porous, non-toxic, and biocompatibility [14]. Polyvinylpyrrolidone (PVP) is an aqueous polymer compound, which is used to stabilize and provide protection to new composite material as well as a dispersant [15].

AgNPs/AC-CTS-PVA gels were synthesized in the present study. Fourier transform infrared spectroscopy (FT-IR), X-ray diffraction (XRD), Scanning electron microscopy (SEM) and Thermogravimetry as well as differential thermal analysis (TGA-DTA) were used to characterize the composite. The gel was tested regarding antibacterial activity against Pseudomonas aeruginosa, Staphylococcus aureus as well as the synergistic effect of antibacterial activity of C-Ag and CTS. The data of the dye adsorption experiment were analyzed using quasi-first order kinetic equation and quasi-

second order kinetic equation. Moreover, reusability, long term stability and antibacterial effect of the gel at various pH were studied. PVA and CTS were tested on the gel expansion, rate of water loss, water content, water adsorption and degradation. The maximum adsorption capacity of the material was tested by the construction of kinetic models. The gel materials, which are good in their antimicrobial qualities, desirable physical traits and adsorption, are good to use in the sewage treatment.

MATERIALS AND METHODS

Materials

Chitosan (viscosity 1 %, deacetylation 80 %) and Polyvinylpyrrolidone were purchased from Otto Chemie Private Limited, Mumbai, India. Polyvinyl Alcohol was acquired from SDFCL pvt. Ltd., India. Formicacid and ethanol were acquired from Molychem pvt. Ltd., India. Vitamin C (Ascorbic acid) and silver nitrate were purchased from Merck Chemicals, India. Sodium carbonate was purchased from Rankem, India. Methylene blue dye known as methylthioninium chloride ($C_{16}H_{18}N_3SCl.3H_2O$) was purchased from Merck, India. Calcium carbonate and boric acid were also purchased from the local market in India. The waste water chestnut stems were collected from a pond in Bareilly, India. Double distilled water was used in all studies.

Preparation of C-Ag

Water chestnut stem (WCS) were washed with clean water to remove dirt and water soluble impurities and dried in sun light. After drying, water chestnut stem were grinded. The powder of water chestnut stem were calcined in a muffle furnace at 300 °C for 120 min, under N_2 atmosphere and after carbonization, the powder of water chestnut stem were removed. 4 g of carbonized water chestnut stem powder was added to 40 ml of silver nitrate solution and stirred for 4 hours. Silver ions were reduced by adding ascorbic acid (0.40 g) to the above solution, soaked for overnight, filtered and dried in vacuum oven for 12 hours at 50°C temperature. Subsequently, the water chestnut stem biochar was placed in a muffle furnace and heated for 2 hours at 300 °C. Finally, the C-Ag composite was obtained.

Preparation of AgNPs/AC-CTS-PVA Gels

0.1 g of chitosan was dissolved in 10 mL double distilled water (0.1 mL formic acid) with constant stirring and 0.25 g of polyvinyl alcohol was dissolved in 25 mL double distilled water with constant stirring. 0.02 g polyvinylpyrrolidone was added in polyvinyl alcohol solution and mixed well. Above both solutions were mixed well and 0.25 g C/Ag was added with continuous stirring for 4 hours. After that 0.1 g $CaCO_3$ powder was blended with 1 ml absolute ethanol. The mixture was continuously heated at 80 °C for 30 minute and stirred until ethanol was fully evaporated. Immediately 0.1 g boric acid was added for cross-linking for 30 minute. After that the above mixture was dropped into 10 wt % Na_2CO_3 solution and left overnight, and excessive Na_2CO_3 was washed with deionized water. Finally, the gels were dried under the temperature of 50 °C in a vacuum oven to obtain AgNPs/AC-CTS-PVA gels.

Antimicrobial Assay

The antimicrobial activity of AgNPs/AC-CTS-PVA and chitosan (CTS) were assessed using the agar well diffusion technique. The test organisms included both Gram-positive and Gram-negative bacteria: *Staphylococcus aureus* (MTCC 3160), and *Pseudomonas aeruginosa*. Nutrient broth was prepared and sterilized at 121 °C for 15 minutes to ensure aseptic conditions. Each bacterial strain was cultured overnight in the nutrient broth to obtain active inocula [16]. Fresh Mueller-Hinton Agar (MHA) plates were filled and left to solidify after which the 24 hour old bacterial cultures were then evenly distributed on the agar plates. Five millimeter diameter wells were then punched through the agar and 50 µL of each test sample dispensed into the wells. The incubation of plates at 37°C was done over 24 hours, and the efficacy of antimicrobials was found by measuring the diameter of the inhibitory zones around the well [17, 18]. All tests were performed in triplicate to ensure reproducibility. Penicillin was used as a standard antibiotic control to benchmark the antimicrobial potency of the tested samples, with all compounds prepared at 1 mg/mL concentration in pH 7.0 buffer solution prior to the assay.

Dye Adsorption Studies

The AgNPs/AC-CTS-PVA were used to study the adsorption behavior of cationic dye methylene blue [19]. The known weight of the nano-composite (AgNPs/AC-CTS-PVA) sample was put into the solution of different concentration of methyl blue for 1 hour. After filtration the AgNPs/AC-CTS-PVA were dried. Methyl blue is a cationic dye, which was used as a model dye to evaluate the adsorption capacity of AgNPs/AC-CTS-PVA. The Methyl blue dye removal experiment was conducted in 25 ◦C temperature. In this experiment, 100 mg of the Methyl blue dye was dissolved in 1 L of double distilled water and the pH of the dye solution was adjusted by adding HCl or NaOH. The required amount of AgNPs/AC-CTS-PVA was added to the 10 mL dye solution and stirred for optimum time and this experiment was analyzed at the wavelength (λ_{max}) 665 nm using UV-Vis spectrophotometer to calculate the residual dye concentration. The dye adsorption capacity was calculated as follows [20,21].

$$\text{Dye Adsorption (q)} = \frac{\text{Co}-\text{Ce}}{\text{W}} \text{x V}$$

Where Co is the initial concentration of dye, Ce is the final concentration of dye, V is volume, W is the weight of crosslinking sample.

Optimization of Various Adsorption Conditions

The methylene blue (MB) adsorption by AgNPs/AC-CTS-PVA was investigated by varying only one adsorption parameter at a time while others kept fixed. Various adsorption parameters and their range pH (2 to 8), adsorbent dose (10 mg-50 mg), temperature (10°C to 60°C), contact time 60 minutes and contact volume 10 mL at 100 ppm of methylene blue dye were studied [22].

Adsorption Isotherm Studies

For isotherm investigation, the adsorption equilibrium data was originated at different initial MB concentrations ranging from 100 ppm to 400 ppm using 20 mg of the AgNPs/AC-CTS-PVA, contact time 60 minutes at pH 7 with 10 mL MB dye solution at room temperature.

Adsorption Isotherm

The Langmuir isotherm assumes monolayer adsorption on a homogeneous surface with finite and identical adsorption sites [23]. The linear Langmuir equation is expressed as:

$$\frac{\text{Ce}}{\text{Qe}} = \frac{1}{\text{QmKL}} + \frac{\text{Ce}}{\text{Qm}} \quad (1)$$

The Freundlich isotherm describes adsorption on heterogeneous surfaces and is expressed as:

$$\ln Qe = \ln KF + \frac{1}{\text{n}} \ln Ce \quad (2)$$

Kinetic Studies

In order to investigate kinetic data, the interaction time was varied from 10 to 90 minutes and the kinetic studies were completed by using 100 ppm MB dye concentration, 20 mg adsorbent dose at pH 7 and temperature 25 °C. There are six kinetic models, namely first order, pseudo first order, second order and pseudo second order, was used to describe the mechanism of adsorption kinetics [24-26].

The linear form first order is given as equation (3).

$$\ln \frac{\text{Qo}}{\text{Qt}} = \text{k}_1\text{t} \quad (3)$$

Lagrange equation in integrated form is given in equation (4).

$$\log \frac{(\text{Qo}-\text{Qt})}{\text{Qo}} = \log \text{Qo} - \frac{\text{k}_1\text{t}}{2.303} \quad (4)$$

The linear form of the second order rate equation is given in equation (5)

$$\frac{1}{(\text{Qo}-\text{Qt})} = \frac{1}{(\text{Qo})} + \text{k}_2\text{t} \quad (5)$$

The pseudo-second-order kinetic rate expression in the integrated form is defined as equation (6)

$$\frac{t}{Qt} = \frac{t}{k_2 Qe^2} + \frac{t}{Qe} \quad (6)$$

This model (intraparticle diffusion) identifies diffusion-controlled adsorption steps (7).

$$Qt = Kid^{0.5} + C \quad (7)$$

The Elovich model is suitable for adsorption on heterogeneous surfaces (8).

$$Qt = \frac{1}{\beta}\ln(\alpha\beta) + \frac{1}{\beta}\ln(t) \quad (8)$$

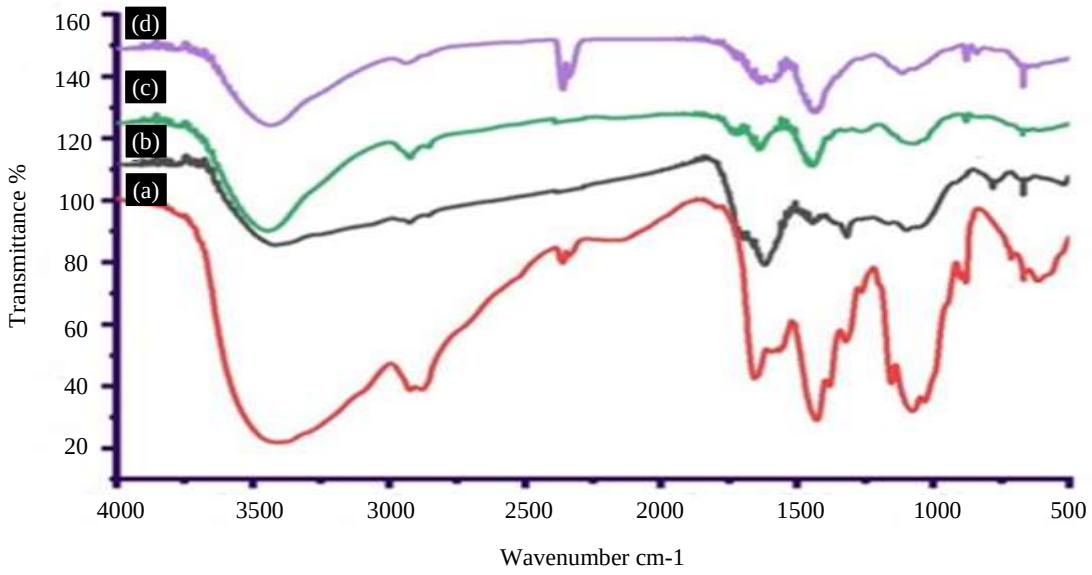

Figure 1. FT-IR spectra of the (a) Chitosan, (b) AC (c) PVA (d) AgNPs/AC-CTS-PVA.

RESULTS AND DISCUSSION

Fourier Transform Infrared (FT-IR) Spectrometry Analysis

The FTIR spectra of chitosan (CTS), activated carbon (AC), polyvinyl alcohol (PVA), and the AgNPs/AC-CTS-PVA composite were recorded in the range of 4000-500 cm^{-1} to investigate their functional groups and possible interactions illustrated in Figure 1 [27]. The FTIR spectrum of chitosan (CTS) shows a broad and intense band in the region of 3200-3500 cm^{-1}, which is attributed to the overlapping stretching vibrations of hydroxyl (-OH) and amine (-NH) groups, indicating extensive hydrogen bonding in the polymeric chain [28]. The typical band at approximately 2920 cm^{-1} relates to C-H stretching of aliphatic -CH_2 groups. The absorption band at approximately 1650 cm^{-1} is attributed to amide I (C=O stretching), and the band at an approximate of 1580 cm^{-1} is due to NH bending (amide II). The presence of peaks at 1420-1380 cm^{-1} can be ascribed to -CH bending vibrations, and -CH and C-O stretching vibrations of the polysaccharide backbone, which are strong in the region of1150-1020 cm^{-1} verifies the chemical structure characteristic of chitosan as shown in Figure 1a [29]. The chemical product of the water chestnut, which was activated carbon (AC) at 300°C has a broad band at 3400 cm^{-1} corresponding to surface -OH groups. There are weak absorption bands around the region of ~2920 cm^{-1} which are linked to aliphatic C-H stretching. The observed band of the region of ~1700-1600 cm^{-1} is associated with C=O stretching of the carboxylic, lactone or quinone groups during the activation and carbonization process. Further, the C-O stretching is attributed to the bands in the range of C-O stretching, of about 1200-1000 cm^{-1} vibrations of phenolic, alcoholic, and ether groups, which show the existence of oxygen-containing functional groups on the AC surface as shown in Figure 1b [30]. PVA spectrum is characterized by a strong and broad -OH band at about 3300-3500 cm^{-1} hydrogen bonded hydroxyl groups. The characteristic C-H vibration of -CH_2- groups is observed at a stretch, at

2940-2910 cm^{-1}. Bands around ~1420-1380 cm^{-1} correspond to $–CH_2$ bending, while the prominent absorption in the region of ~1140-1080 cm^{-1} is assigned to C-O stretching vibrations, confirming the semi-crystalline nature of PVA as shown in Figure 1c [31]. The FTIR spectrum of the AgNPs/AC-CTS-PVA composite (Figure 1d) shows noticeable shifts and reduced intensities of the -OH and C=O related bands compared to pristine PVA and AC. These changes indicate strong intermolecular interactions and coordination between Ag nanoparticles and oxygen-containing functional groups of AC and PVA. The retention of major characteristic bands confirms the structural integrity of the polymer matrix, while the spectral modifications validate the successful formation of the AgNPs/AC-CTS-PVA composite.

X-Ray Diffraction (XRD) Analysis

The crystalline nature and structural changes of chitosan, AgNPs/AC-CTS-PVA composite and dye loaded AgNPs/AC-CTS-PVA composite were investigated in Figure 2 by X-ray diffraction (XRD) analysis in the 2θ range of 10-80°. The XRD curve of chitosan has a wide and strong peak at $2\theta \approx 19.21°$, which is typical of semi-crystalline structure of chitosan (Figure 2a) (32). This maximum is because of intermolecular hydrogen bonding between -OH and $–NH_2$ groups in the polymer chains. The width of the peak implies the domination of an amorphous phase and a small amount of crystalline ordering, which is characteristic of chitosan-based biopolymers. The XRD pattern of AgNPs/AC-CTS-PVA composite reveals a substantial decrease in the intensity of the polymer chain-related broad peak, which is a sign of the disorganization of the polymer chains because of the addition of the activated carbon and silver nanoparticles shown in Figure 2b. Moreover, the observed distinct diffraction peaks at approximately $2\theta \approx 38°$, 44°, 64°, and 77° can be indexed to the (111), (200), (220), and (311) crystallographic planes of face-centered cubic (fcc) structured metallic silver (Ag), respectively [33]. These peaks validate the effective formation and crystalline state of Ag nanoparticles in the AC-PVA matrix. The lack of impurities peaks indicates high purity of the produced Ag nanoparticles. The activated carbon is the primary contributor to the amorphous background as indicated by the broad hump instead of sharp diffraction peaks. The XRD pattern of the dye/AgNPs/AC-CTS-PVA composite still has the typical diffraction peaks of Ag nanoparticles, albeit with a lower intensity and a slight broadening of the peaks depicted in Figure 2c. This action indicates effective adsorption or entrapment of dye molecules in the composite matrix without any crystalline structure changes in Ag nanoparticles. The decrease in peak intensity may be attributed to surface coverage of Ag nanoparticles and AC pores by dye molecules, as well as increased amorphization of the composite system after dye loading and results confirm the semi-crystalline nature of chitosan, the successful incorporation of crystalline Ag nanoparticles within the AC-PVA matrix, and the effective dye loading onto the AgNPs/AC-CTS-PVA composite without destroying its structural integrity [34].

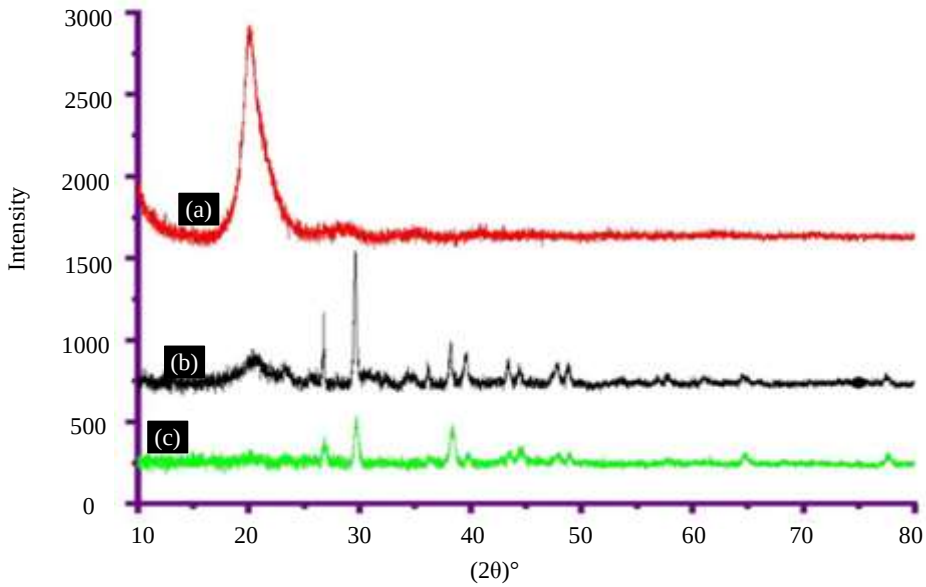

Figure 2. XRD spectra of the (a) Chitosan (b) AgNPs/AC-CTS-PVA (c) Dye/AgNPs/AC-CTS-PVA.

SEM Analysis

The surface morphology of chitosan, activated carbon (AC), AgNPs/AC-CTS-PVA composite, and dye-loaded AgNPs/AC-CTS-PVA composite was examined using scanning electron microscopy (SEM), and the representative micrographs are shown in Figure 3 (a–d). The SEM image of chitosan (Figure 3a) reveals a relatively dense, compact, and flaky surface morphology with irregular plate-like structures and visible cracks [35]. Activated carbon (AC) of water chestnut under the SEM micrograph (Figure 3b) exhibits a very rough, heterogeneous and fragmented surface with irregular shaped particles (30). The morphology of the SEM image of the AgNPs/AC-CTS-PVA composite (Figure 3c) is quite different in relation to the pristine AC and chitosan. The surface proves to be very heterogeneous and agglomerated clusters are incorporated in the polymeric structure. It is worth noting that nanostructures of Ag nanoparticles of shape of a needle and a flower are identified [36], which means that the nucleation and growth of Ag nanoparticles on the AC-PVA framework were successful. As a stabilizing and binding agent, the PVA matrix causes the uniform distribution of Ag nanoparticles and avoids excessive aggregation. The rough and textured surface further suggests strong interfacial interactions among Ag-NPs, activated carbon, and PVA [37]. The dye/AgNPs/AC-CTS-PVA composite (Figure 3d) shows a comparatively smoother and more compact surface morphology. The pores and surface irregularities observed in the unloaded composite are partially covered or filled, indicating successful adsorption or encapsulation of dye molecules within the composite matrix. The agglomeration appears slightly increased, which can be attributed to dye molecules occupying surface active sites and pores of AC and interacting with the polymer matrix.

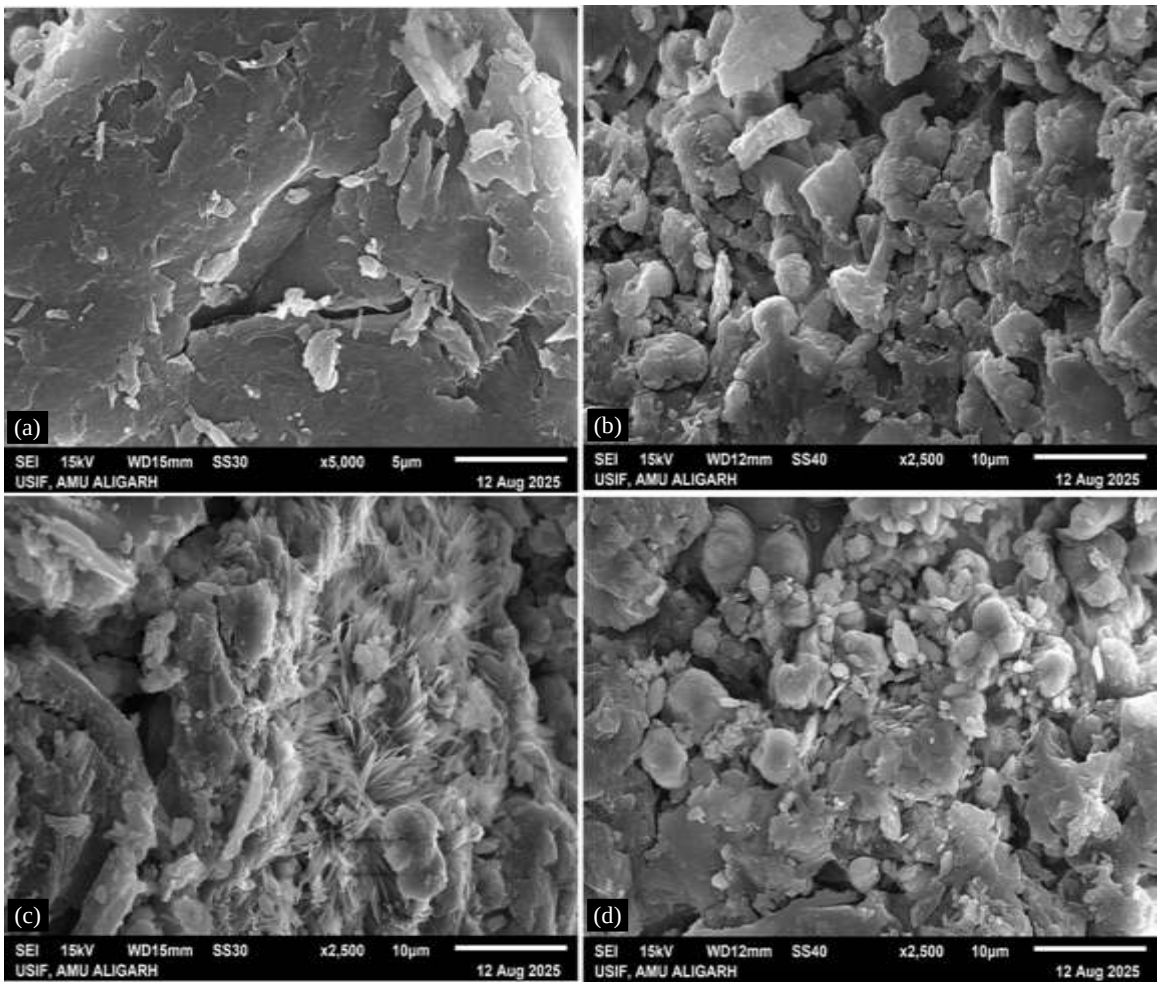

Figure 3. SEM images of the (a) Chitosan (b) AC (c) AgNPs/AC-CTS-PVA (d) Dye/AgNPs/AC-CTS-PVA.

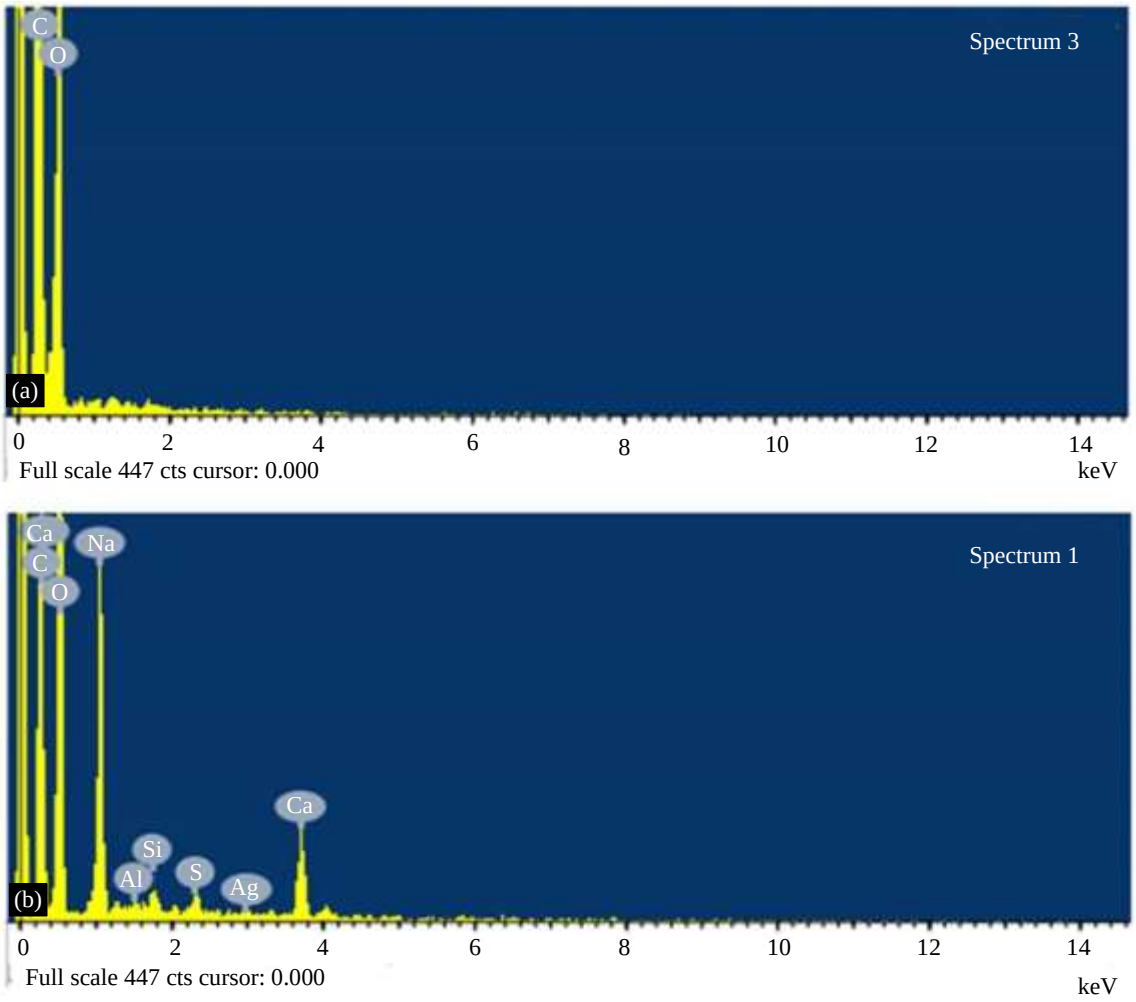

Figure 4. SEM- EDX images of the (a) Chitosan (b) AgNPs/AC-CTS-PVA.

SEM-EDX Analysis

The elemental composition of chitosan and the AgNPs/AC-CTS-PVA composite was analyzed by SEM-EDX, as shown in Figure 4 (a) and (b). The EDX spectrum of the chitosan (Figure 4a) reveals that it is a polysaccharide with carbon (C) and oxygen (O) as dominant elements, and no metallic elements are present [38]. Conversely, AgNPs/AC-CTS-PVA composite (Figure 4b) has a high C and O signal attributed to the activated carbon and the PVA matrix. A clear silver (Ag) peak can be seen, which proves the successful formation and integration of Ag nanoparticles into the composite. Na, Ca, Si, Al, and S minor peaks are also observed, which are probably due to the biomass precursor or the activating agents left over, which also indicates the formation of composite [39].

Thermogravimetric (TGA) Analysis

The thermogravimetric analysis (TGA) and derivative thermogravimetry (DTG) were used to assess the thermal stability and decomposition behaviour of chitosan and the AgNPs/AC-CTS-PVA composite at different temperatures (25-800 °C) as illustrated in Figure 5 (a) and (b), respectively. In the TGA curve of chitosan (Figure 5a) three steps weight loss pattern are observed. The preliminary weight loss of about 12% that was seen beneath 120 °C is ascribed to the loss of physically adsorbed moisture and bound water molecules by the hydrophilic property of chitosan [40]. The second weight loss step takes place at the temperature of between 220 and 350 °C as shown by a strong DTG peak at the temperature range of about 280 to 300 °C. The step is associated with the thermal destruction of the chitosan backbone that encompasses depolymerization, drying of saccharide rings, and breaking down of amine

and acetylated units. Beyond -350 C to 700 °C is the third weight loss step that is linked to additional decomposition of carbonaceous residues and creation of char. In contrast, the AgNPs/AC-CTS-PVA composite (Figure 5b) exhibits enhanced thermal stability with a distinct degradation profile. The initial weight loss below ~150 °C is attributed to the removal of moisture and volatile components from the composite. The second major weight-loss region observed between ~200 and 400 °C corresponds to the degradation of PVA chains, including elimination of hydroxyl groups and chain scission [41]. A further gradual weight loss in the range of ~400-600 °C is related to the decomposition of residual polymeric components and partial oxidation of the carbonaceous framework. Notably, the composite shows a significantly higher residual mass at 800 °C compared to chitosan, which can be attributed to the presence of thermally stable activated carbon and metallic silver nanoparticles.

ADSORPTION STUDIES

The Influence of Adsorbent Dose on the Adsorption of Methylene Blue Dye

Various amounts of polymeric composite (10-50 mg) were added to 10 mL of synthetic dye solution and the mixture was stirred at room temperature for 60 min., after that mixture was centrifuged and filtered. The filtrate was analyzed through UV-Vis spectrophotometer to calculate the conc. methylene blue dye Figure 6a showed that the percentage of removal of methylene blue dye reached about 98 % with a dosage of 20 mg of the polymeric composite, further increase in dosage resulted in approximately the same removal efficiency [42].

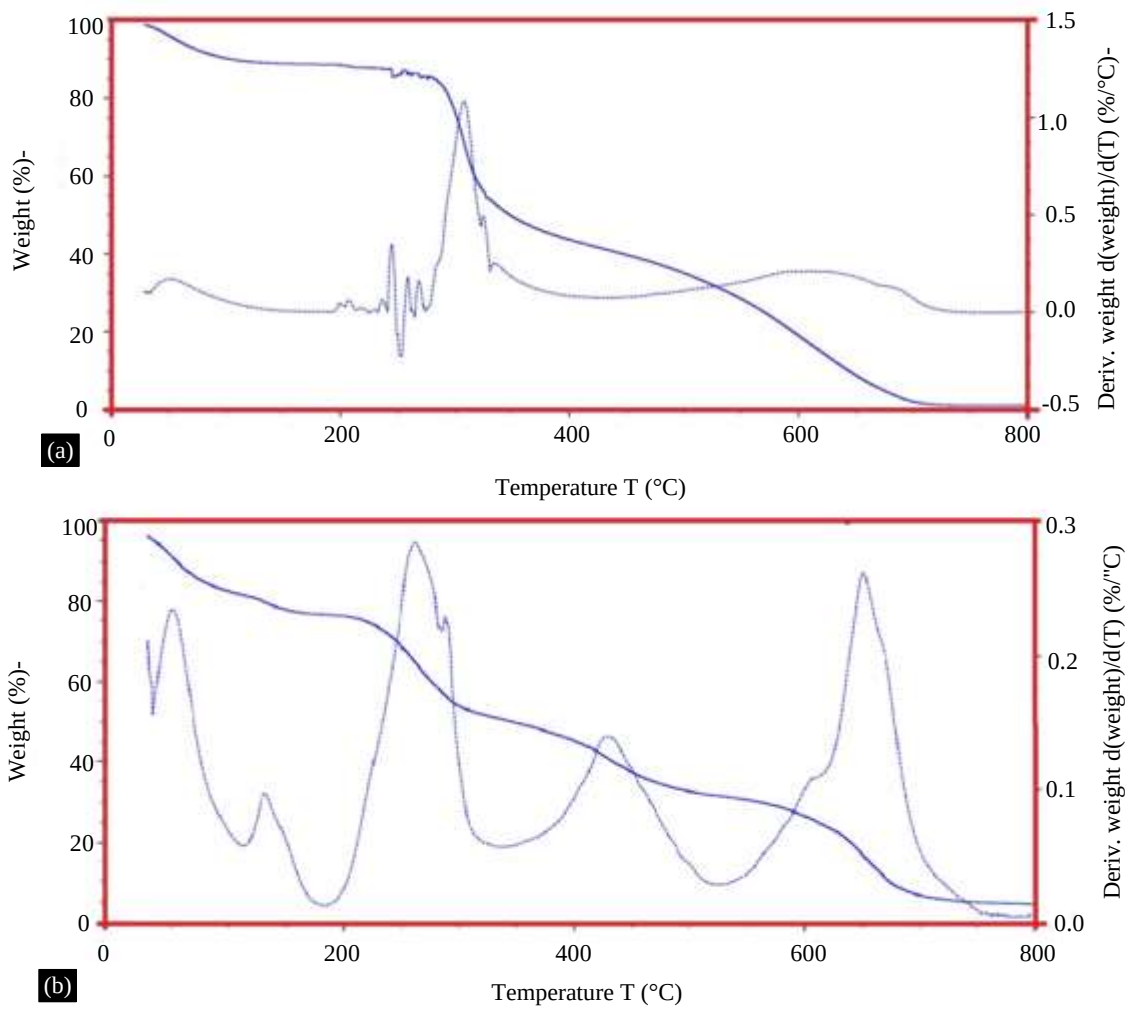

Figure 5. TGA curves of the (a) Chitosan (b) AgNPs/AC-CTS-PVA.

The Impact of pH on the Adsorption of Methylene Blue Dye

The impact of pH on the sorption of methylene Blue by the polymeric composite was shown in Figure 6b. The data demonstrated a relative decrease in methylene blue adsorption in an acidic medium as well as basic medium. The adsorption of methylene blue increased, as the pH increased from 1 to 7 pH. Beyond pH 7 the adsorption of methylene blue decreased. At pH 7, strong electrostatic interactions were generated between the active functional group of polymeric composite and methylene blue, resulting in maximum adsorption capacity of the polymeric composite at pH 7 [43].

The Influence of Time on the Adsorption of Methylene Blue Dye

The impact of contact time was studied by changing the equilibrium time from 10 to 100 min at room temperature and near-neutral pH for methylene Blue adsorption onto the polymeric composite. Figure 6c clearly demonstrated that the adsorption rate of methylene blue dye gradually increased from 10 to 60 min. afterword increasing the contact time from 60 to 100 min the adsorption reached equilibrium [44].

The Influence of Temperature on the percent Adsorption of Methylene Blue Dye

The influence of temperature on the percent adsorption of Methylene Blue as shown in Figure 6d. The percentages of dye adsorption increased gradually from 90 to 98 % with the increase in temperature from 10 to 30 °C and increasing the temperature from 30-60 °C resulted in nearly constant adsorption [45].

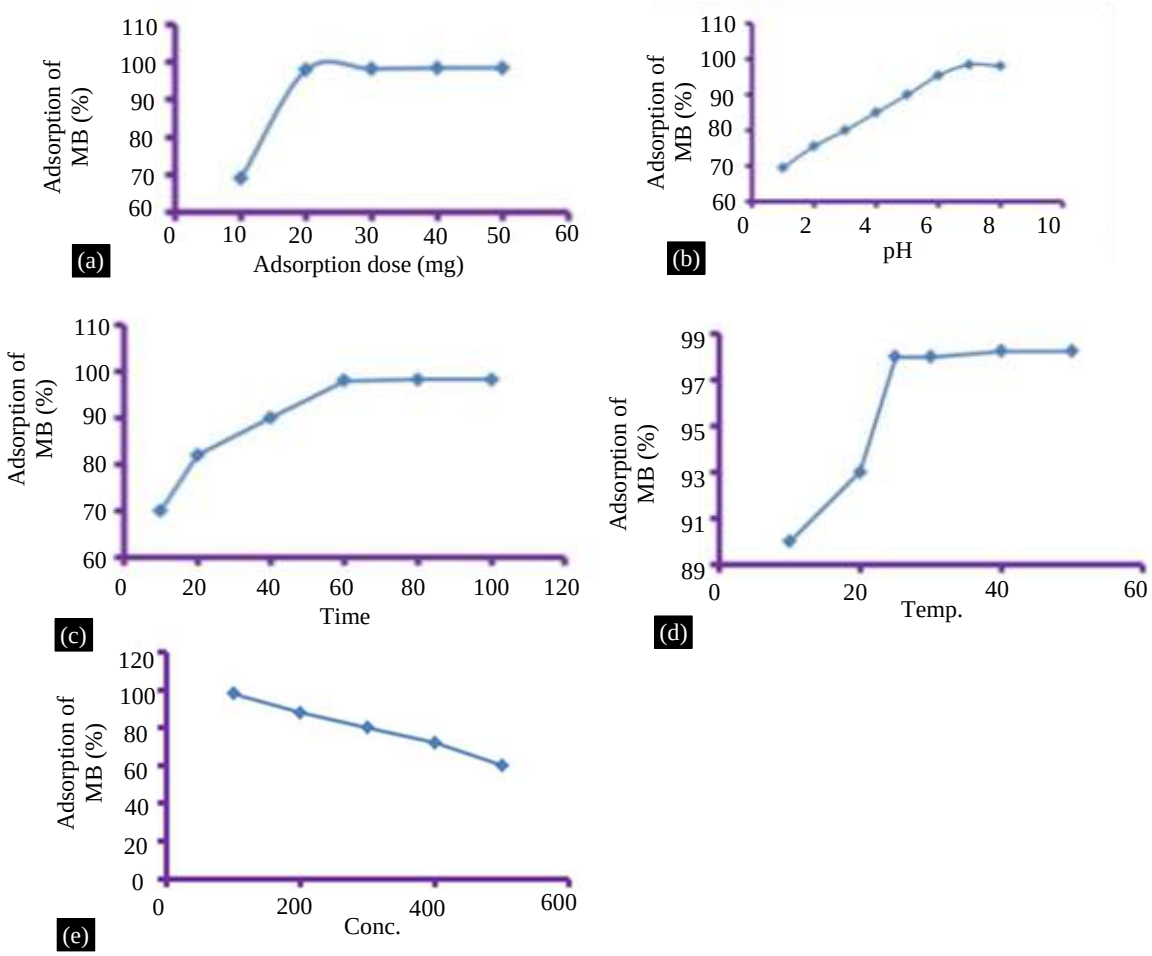

Figure 6. (a) Effect of Adsorbent Dose on the Methylene Blue Dye Adsorption (b) Effect of pH on the Methylene Blue Dye Adsorption (c) Effect of Time on the Methylene Blue Dye Adsorption (d) Effect of Temperature on the Methylene Blue Dye Adsorption (e) Effect of Methylene Blue Dye Initial Concentrationson the Methylene Blue Dye Adsorption.

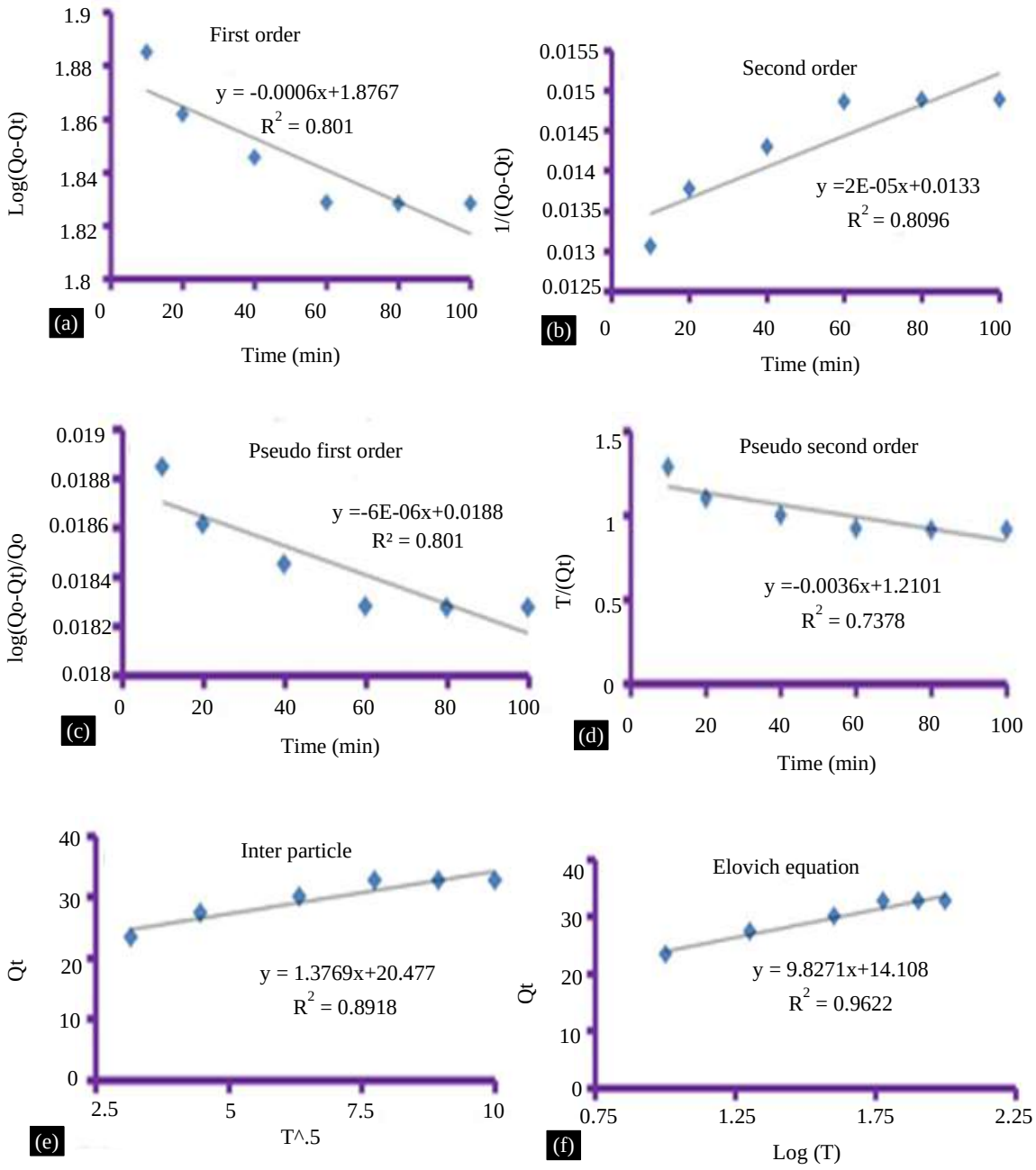

Figure 7. (a) First Order, (b) Second Order (c) Pseudo-Second Order (d) Pseudo-Second Order (e) Inter Particle and (f) Elovich Kinetic Model for the Adsorption of MB by the Adsorbent.

Table 1. Kinetic model parameters.

S.N.	Model	Slope	Intercept	Calculated parameters	R^2
1	First order	–0.0006	1.8767	$k_1 = 0.0006\ min^{-1}$	0.801
2	Second order	2×10^{-5}	0.0133	$k_2 = 2 \times 10^{-5}$	0.8096
3	Pseudo-first order	-6×10^{-6}	0.0188	$k_1 = 6 \times 10^{-6}\ min^{-1}$	0.801
4	Pseudo-second order	–0.0036	1.2101	$k_2 = -0.0036\ g\ mg^{-1}\ min^{-1}$; $q_e(calc) = 0.826\ mg\ g^{-1}$	0.7378
5	Intra-particle diffusion	1.3769	20.477	$k_i d = 1.3769\ mg\ g^{-1}\ min^{-½}$; C = 20.477	0.8918
6	Elovich	9.8271	14.108	α = 14.108; β = 9.8271	0.9622

The Influence of Methylene Blue Initial Concentrations

The impact of the initial methylene Blue concentration on the adsorption of dye onto polymeric composite at near-neutral pH and at room temperature was studied by changing the initial concentration of methylene blue dye in the range of 100 to 500 ppm [46]. The influence of methylene blue dye concentration on adsorption was shown in Figure 6e. According to the experimental results, adsorption increased when increasing the concentration methylene blue dye from 100 ppm to 500 ppm.

Kinetic Modeling of Adsorption

The adsorption kinetics was evaluated using first-order, second-order, pseudo-first-order, pseudo-second-order, intra-particle diffusion, and Elovich models shown in Table 1 and Figure 7. The linear regression coefficients indicate that the adsorption process does not follow a simple single-step mechanism. The first-order and pseudo-first-order models showed moderate correlation (R^2 = 0.801), whereas the second-order model exhibited slightly improved fitting (R^2 = 0.8096). The pseudo-second-order model presented comparatively lower linearity (R^2 = 0.7378), suggesting that chemisorption is not the sole rate-controlling step. The intra-particle diffusion model demonstrated good linearity (R^2 = 0.8918), indicating that pore diffusion significantly contributes to adsorption. However, the non-zero intercept (C = 20.477) confirms that intra-particle diffusion is not the only rate-limiting mechanism and that boundary layer diffusion also plays a role. The Elovich equation had the largest correlation coefficient (R^2 = 0.9622), which implies that the adsorption was on a heterogeneous surface with chemisorption properties. On the whole, the adsorption process can be regulated by a combination of several mechanisms, which require interaction with the surface and diffusion processes [24-26].

Adsorption Isotherm Study

The Langmuir and Freundlich isotherm models were used to analyze the equilibrium adsorption data shown in Table 2 and Figure 8. The Langmuir model showed high linearity (R^2 = 0.9938), which indicated that monolayer adsorption was taking place on a uniform surface with the same binding sites. The adsorption capacity ($Q_{\square}$) was estimated to be 106.38 mg g^{-1}, which showed that the adsorbent prepared was very efficient in adsorption. A strong adsorbate-adsorbent affinity is indicated by the Langmuir constant (K_L = 0.0745 L mg^{-1}). Freundlich model also displayed a high correlation (R^2 = 0.9898), which means that there is some level of surface heterogeneity. Favorable adsorption (n -1) (n = 3.92) is proven by the Freundlich constant (K_F = 27.28 mg g^{-1} (L $mg^{-1})^{1/n}$) and the adsorption intensity (n). The slightly increased R^2 of the Langmuir model indicates to a relatively greater extent that in the case of monolayer adsorption, but with small heterogeneous surface interactions [47].

Table 2. Isotherm model parameters.

S.N.	Model	Parameter	Value	R^2
1	Langmuir	$Q_{\square}$ (mg g^{-1})	106.38	0.9938
		K_L (L mg^{-1})	0.0745	
2	Freundlich	K_F (mg g^{-1} (L $mg^{-1})^{1/n}$)	27.28	0.9898
		N	3.92	

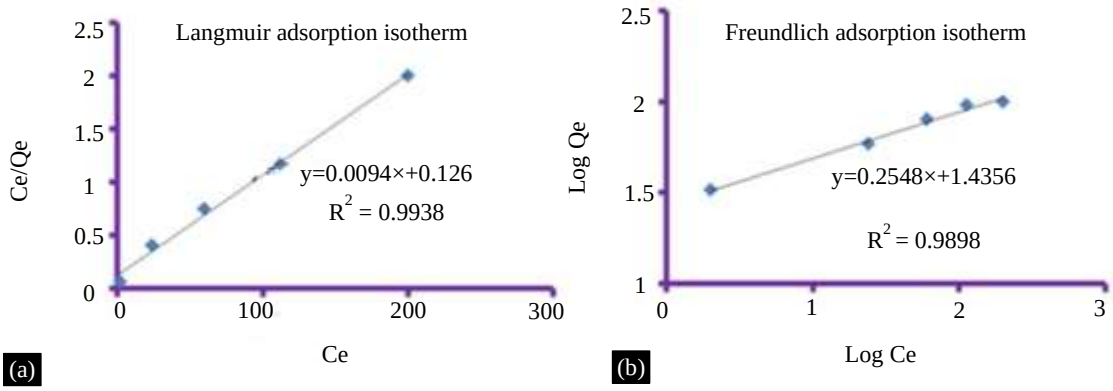

Figure 8. (a) Langmuir Adsorption isotherm (b) Freundlich Adsorption.

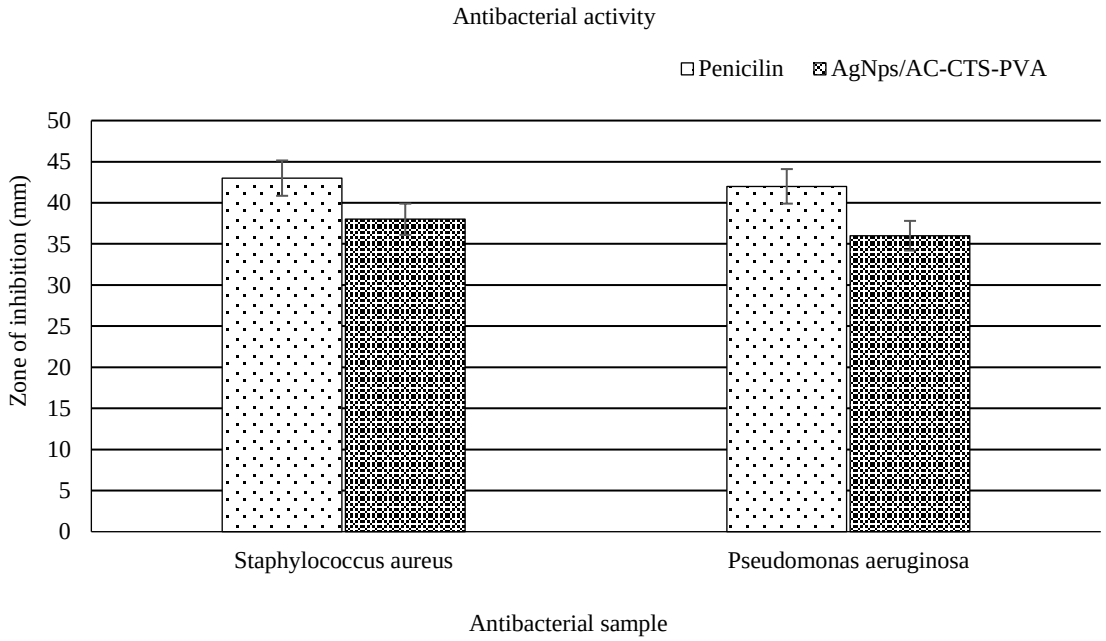

Figure 9. Represent the antibacterial activity of AgNPs/AC-CTS-PVA against staphylococcus aureus and pseudomonas aeruginosa.

Antibacterial Activity

The antimicrobial effect of the developed nanocomposites (AgNPs/AC-CTS-PVA) were assessed against staphylococcus aureus and pseudomonas aeruginosa by agar well diffusion technique where penicillin was used as the standard reference drug and blank control (without any sample) was taken (Figure 9). In the control sample, a zone of inhibition (0 mm) was not observed and it was confirmed that there was no intrinsic antibacterial activity in the blank medium [48]. Conversely, penicillin had a strong antibacterial effect as it had a zone of inhibition of about 42 mm and it was much bactericidal. AgNPs/AC-CTS-PVA composite was also found to be highly antibacterial, with a zone of inhibition of about 38 mm with staphylococcus aureus, similar to the standard antibiotic. A zone of 36 mm was also observed in pseudomonas aeruginosa that also demonstrated a significant antibacterial activity [49]. The fact that the inhibition zone was low, when compared to penicillin, is an indicator of high antimicrobial efficacy of the synthesized composite, which can probably be explained by the synergistic effect of silver nanoparticles and the polymeric matrix. The good antibacterial activity can be linked to the liberation of Ag+ ions, cell membrane destabilization, and the interaction with intracellular biomolecules resulting in the death of the cell [50]. These findings validate the idea that AgNPs/AC-CTS-PVA composite has good antibacterial potential and can be an effective antimicrobial material.

CONCLUSION

In this work, a green and sustainable AgNPs functionalized activated carbon/chitosan-PVA (AgNPs/AC-CTS-PVA) composite gel was effectively produced using water chestnut stem-derived biochar in dual wastewater treatment and antibacterial purposes. Structural and morphological methods (FTIR, XRD, SEM-EDX, and TGA) were used to verify proper insertion of crystalline silver nanoparticles into the polymeric structure and to prove enhanced thermal stability and structural integrity of the composite. The material obtained was found to be highly adsorbing to the methylene blue (MB) dye with a maximum removal efficiency of about 98% at optimal conditions (pH 7, 20 mg dose, 60 min). Kinetic analysis showed that the adsorption mechanism was best elucidated by the Elovich model (R^2 = 0.9622), which indicated that the mechanism was mainly achieved through heterogeneous chemisorption, and that intra-particle diffusion also played a role. The isotherm analysis showed that the Langmuir model (R^2 = 0.9938) was strictly followed with maximum adsorption

capacity ($Q_{\square}$ = 106.38 mg g^{-1}) indicating that most of the adsorption is monolayer. Moreover, the composite showed impressive antimicrobial properties against Staphylococcus aureus with a 40 mm inhibition zone that was similar to penicillin (42 mm). Altogether, the designed AgNPs/AC-CTS-PVA gel is a potential, versatile material to apply in the effective dye removal and antimicrobial treatment of wastewater.

Acknowledgement

Mohattib Ali is very thankful to the Mahatma Jyotiba Phule Rohilkhand University, Bareilly (UP) for the financial support in the form of a Teaching Assistantship (TA) to carry out this work.

REFERENCES

1. Thamer A, Mustafa A, Bashar H, Van B, Le P-C, Jakab M, et al. Activated carbon and their nanocomposites derived from vegetable and fruit residues for water treatment. Journal of Environmental Management. 2024;359:121058.
2. Kumar P, Gihar S, Kumar B, Kumar D. Synthesis and characterization of crosslinked chitosan for effective dye removal antibacterial activity. International journal of biological macromolecules. 2019;139:752-9.
3. Zhang Z, He Y-C, Liu Y. Efficient antibacterial and dye adsorption by novel fish scale silver biochar composite gel. International Journal of Biological Macromolecules. 2023;248:125804.
4. Kumari S, Poonia A. Formulation and characterization of antioxidants rich tablets using Trapa natans L. peel extract. Food and Humanity. 2025:100951.
5. Kharbanda C, Alam MS, Hamid H, Bano S, Haider S, Nazreen S, et al. Trapa natans L. root extract suppresses hyperglycemic and hepatotoxic effects in STZ-induced diabetic rat model. Journal of ethnopharmacology. 2014;151(2):931-6.
6. Obayomi KS, Lau SY, Ibrahim O, Zhang J, Meunier L, Aniobi MM, et al. Removal of Congo red dye from aqueous environment by zinc terephthalate metal organic framework decorated on silver nanoparticles-loaded biochar: mechanistic insights of adsorption. Microporous and Mesoporous Materials. 2023;355:112568.
7. Dalmaz A, ÖZAK SS. Methylene blue dye efficient removal using activated carbon developed from waste cigarette butts: Adsorption, thermodynamic and kinetics. Fuel. 2024;372:132151.
8. Senthilkumar K, Kamalraj T, Keerthana P, Ramesh S, Naveenkumar M. Activated carbon derived from fish gill waste. Materials Chemistry and Physics. 2024;328:129990.
9. Khan N, Kumar D, Kumar P. Silver nanoparticles embedded guar gum/gelatin nanocomposite: Green synthesis, characterization and antibacterial activity. Colloid and Interface Science Communications. 2020;35:100242.
10. Feng Q, Fan B, He Y-C, Ma C. Antibacterial, antioxidant and fruit packaging ability of biochar-based silver nanoparticles-polyvinyl alcohol-chitosan composite film. International Journal of Biological Macromolecules. 2024;256:128297.
11. Kumar D, Gihar S, Shrivash MK, Kumar P, Kundu PP. A review on the synthesis of graft copolymers of chitosan and their potential applications. International Journal of Biological Macromolecules. 2020;163:2097-112.
12. Kumar P, Khan N, Kumar D, Ali M, Tandon R. Microwave-assisted synthesis of curcumin-encapsulated silica-chitosan composite for drug release study. Bulg Chem Commun. 2023;55:102-8.
13. Chikkegowda A, Raj LA, Vaishnavi N, Mohan SB, Krishnaveni S. Gamma Ray Interaction studies on Light-weight, Eco-Friendly PVA-Based Composites Using Construction Waste materials as Fillers. Applied Radiation and Isotopes. 2025:112356.
14. Fatima M, Mir S, Awwad NS, Ibrahium HA. Green approach for removal of crystal violet dye using silane crosslinked and clay reinforced chitosan/polyvinyl pyrrolidone nanocomposite. Journal of Molecular Liquids. 2025;436:128230.

15. Hu Z, Zhang L, Zhong L, Zhou Y, Xue J, Li Y. Preparation of an antibacterial chitosan-coated biochar-nanosilver composite for drinking water purification. Carbohydrate Polymers. 2019;219:290-7.
16. Díez-Pascual AM. State of the art in the antibacterial and antiviral applications of carbon-based polymeric nanocomposites. International Journal of Molecular Sciences. 2021;22(19):10511.
17. Demirel MH, Gül A, Aydoğmuş E, Özgen İ, Arslanoğlu H. Antibacterial efficacy of pyrolysis-derived plant fractions against resistant pathogens: a comparative evaluation using nutrient and Müller–Hinton agar. Journal of the Science of Food and Agriculture. 2026.
18. Suba V, Saravanabhavan M, Krishna LS, Kaleemulla S, Kumar ER, Rathika G. Evaluation of curcumin assistance in the antimicrobial and photocatalytic activity of a carbon based TiO 2 nanocomposite. New Journal of Chemistry. 2020;44(37):15895-907.
19. Li Y, Du Q, Liu T, Peng X, Wang J, Sun J, et al. Comparative study of methylene blue dye adsorption onto activated carbon, graphene oxide, and carbon nanotubes. Chemical Engineering Research and Design. 2013;91(2):361-8.
20. Pathania D, Sharma S, Singh P. Removal of methylene blue by adsorption onto activated carbon developed from Ficus carica bast. Arabian journal of chemistry. 2017;10:S1445-S51.
21. Altıntıg E, Altundag H, Tuzen M, Sarı A. Effective removal of methylene blue from aqueous solutions using magnetic loaded activated carbon as novel adsorbent. Chemical Engineering Research and Design. 2017;122:151-63.
22. Gottipati R, Mishra S. Process optimization of adsorption of Cr (VI) on activated carbons prepared from plant precursors by a two-level full factorial design. Chemical Engineering Journal. 2010;160(1):99-107.
23. Gihar S, Kumar D, Kumar P. Facile synthesis of novel pH-sensitive grafted guar gum for effective removal of mercury (II) ions from aqueous solution. Carbohydrate Polymer Technologies and Applications. 2021;2:100110.
24. Gomez V, Larrechi MS, Callao MP. Kinetic and adsorption study of acid dye removal using activated carbon. Chemosphere. 2007;69(7):1151-8.
25. Nethaji S, Sivasamy A. Adsorptive removal of an acid dye by lignocellulosic waste biomass activated carbon: equilibrium and kinetic studies. Chemosphere. 2011;82(10):1367-72.
26. Kumar D, Pandey J, Khan N, Kumar P, Kundu PP. Synthesize and characterization of binary grafted psyllium for removing toxic mercury (II) ions from aqueous solution. Materials Science and Engineering: C. 2019;104:109900.
27. Wibawa PJ, Nur M, Asy'ari M, Nur H. SEM, XRD and FTIR analyses of both ultrasonic and heat generated activated carbon black microstructures. Heliyon. 2020;6(3).
28. Kumar D, Kumar P, Pandey J. Binary grafted chitosan film: Synthesis, characterization, antibacterial activity and prospects for food packaging. International journal of biological macromolecules. 2018;115:341-8.
29. Kumar D, Pandey J, Kumar P. Synthesis and characterization of modified chitosan via microwave route for novel antibacterial application. International journal of biological macromolecules. 2018;107:1388-94.
30. Singh A, Himanshu M, Verma B, Singh R, Lal B, Syed A, et al. Evaluation of sustainability of fabrication process and characterization studies of activated carbon nanocatalyst from waste chestnut peels. Journal of Molecular Structure. 2025;1321:139810.
31. Azeez S, Shenbagaraman R. Fourier transform infrared spectroscopy in characterization of bionanocomposites. Characterization Techniques in Bionanocomposites: Elsevier; 2025. p. 209-27.
32. Huang W-C, Zhao D, Guo N, Xue C, Mao X. Green and facile production of chitin from crustacean shells using a natural deep eutectic solvent. Journal of agricultural and food chemistry. 2018;66(45):11897-901.
33. Alam MA, Sadia SI, Shishir MKH, Bishwas RK, Ahmed S, Al-Reza SM, et al. Crystallinity integration and crystal growth behavior study of preferred oriented (111) cubic silver nanocrystal. Inorganic Chemistry Communications. 2025;173:113834.

34. Zhang L, Zheng S, Hu Z, Zhong L, Wang Y, Zhang X, et al. Preparation of polyvinyl alcohol/bacterial-cellulose-coated biochar–nanosilver antibacterial composite membranes. Applied Sciences. 2020;10(3):752.
35. Zhao R, Amstad E. Bio-informed porous mineral-based composites. Small. 2025;21(7):2401052.
36. Eid KA, Azzazy HM. Controlled synthesis and characterization of hollow flower-like silver nanostructures. International Journal of Nanomedicine. 2012:1543-50.
37. Abbas R, Luo J, Qi X, Naz A, Khan IA, Liu H, et al. Silver nanoparticles: Synthesis, structure, properties and applications. Nanomaterials. 2024;14(17):1425.
38. Mohideen MM, Wang Q, Ramakrishna S, Liu Y. Chitosan-derived carbon sphere with self-activating behavior for stable oxygen reduction reaction in acid and alkaline media. Carbon. 2024;226:119154.
39. Aina ST, Kyomuhimbo HD, Ramjee S, Du Plessis B, Mjimba V, Maged A, et al. Synthesis and assessment of antimicrobial composites of Ag nanoparticles or AgNO3 and egg shell membranes. Molecules. 2023;28(12):4654.
40. Taboada E, Cabrera G, Jimenez R, Cardenas G. A kinetic study of the thermal degradation of chitosan-metal complexes. Journal of applied polymer science. 2009;114(4):2043-52.
41. Alhulaybi ZA, Dubdub I. Kinetics study of PVA polymer by model-free and model-fitting methods using TGA. Polymers. 2024;16(5):629.
42. Goswami S, Naik S. Natural gums and its pharmaceutical application. Journal of Scientific and Innovative Research. 2014;3(1):112-21.
43. Przybytniak G. Crosslinking of polymers in radiation processing. Applications of ionizing radiation in materials processing. 2017:249-67.
44. Mane S, Ponrathnam S, Chavan N. Effect of chemical cross-linking on properties of polymer microbeads: A review. Can Chem Trans. 2015;3(4):473-85.
45. Al-Asadi ST, Al-Qaim FF, Al-Saedi HFS, Deyab IF, Kamyab H, Chelliapan S. Adsorption of methylene blue dye from aqueous solution using low-cost adsorbent: kinetic, isotherm adsorption, and thermodynamic studies. Environmental Monitoring and Assessment. 2023;195(6):676.
46. Merklein E, de Freitas AS, Franco RA, Ferreira M. Influence of acid route on chitosan nanoparticle formation: Physicochemical properties and application in methylene blue adsorption. Environmental Nanotechnology, Monitoring & Management. 2026:101122.
47. Yusop MFM, Rashid MM, Alam MM, Ahmad MA. Synthesis of deprotonated-langsat peel activated carbon for improved Pb2+ adsorption: Optimization and F-test for isotherm and kinetic models. Diamond and Related Materials. 2026:113650.
48. Balouiri M, Sadiki M, Ibnsouda SK. Methods for in vitro evaluating antimicrobial activity: A review. Journal of pharmaceutical analysis. 2016;6(2):71-9.
49. Bernardino-Nicanor A, Fernández-Avalos S, González-Cruz L. Thermal treatment increases the antimicrobial activity of tepejilote rachis against Pseudomonas aeruginosa and Staphylococcus aureus. Natural Product Research. 2025:1-5.
50. Madhusudanan M, Zhang J, Pandit S, Singh P, Jeong GJ, Khan F, et al. Green Synthesis of Silver Nanoparticles: A Review of Polymer and Antimicrobial Drug Combinations for Enhanced Antimicrobial Applications. Advanced NanoBiomed Research. 2025;5(12):2400194.

